Supplementary Information for

Nanoscale Plasmon-Exciton Interaction: The Role of Radiation Damping and Mode-Volume in Determining Coupling Strength

*Manish Kumar, Jyotirban Dey, Mrigank Singh Verma and Manabendra Chandra**

Department of Chemistry, Indian Institute of Technology Kanpur, Kanpur-208016, Uttar Pradesh, India

Corresponding Author

*Email: mchandra@iitk.ac.in

Table of Contents

1. Radiation damping dependent linewidth of gold nanorods:

There are four main damping channels which contribute to the homogenous linewidth (γ_p) of any plasmonic nanostructures.[1,2] These channels include bulk dephasing (γ_p^b), radiation damping (γ_p^{rad}), electron-surface scattering (γ_p^{surf}) and chemical interface damping (γ_p^{CID})

$$\gamma_p = \gamma_p^b + \gamma_p^{rad} + \gamma_p^{surf} + \gamma_p^{CID} \tag{1}$$

Bulk dephasing arises due to thermal phonons, electron scattering and impurities. It depends on the material of the nanoparticles, and the LSPR frequency. In the present case, the constituent material as well as the LSPR frequencies of all the nanorods are identical. As a result, the variation in the contribution of bulk dephasing toward the overall plasmon damping on going from NR1 to NR3 is negligible. Now, the contribution of electron surface scattering becomes important only when the nanoparticle dimension (length or diameter) is less than 10 nm.[2] Since, the dimensions (both length and diameter) of NR1-NR3 are much larger than 10 nm, the damping due to electron-surface scattering is insignificant. Chemical interface damping (CID) is a recently proposed excitation damping pathway, which involves the direct transfer of interfacial hot-electron energy from a metal to a chemical entity attached to or adsorbed onto the metallic surface. Clearly, the chemical interface damping is very much dependent on the properties of the molecules adsorbed onto the nanoparticle surface. Moreover, CID is significant and strongly size dependent only when the particle size is less than 20 nm. In the present case, all the nanorods have their dimensions greater than 20 nm, all of them are capped with CTAB and all of them are dispersed in water. Therefore, the contribution of γ_p^{CID} toward total damping (γ_p) is negligible for our nanorods and the contribution should remain constant for NR1 – NR3. Finally, all the three nanorods possess different physical volumes and the variation in particle volume is very wide: 11000 nm^3 (NR1) to 136000 nm^3 (NR3). Such wide variation in physical volumes (in the dimension regime > 20 nm) ensures that the contributions of radiation damping vary significantly from NR1 to NR3.[1] Therefore, it is obvious that the observed variation in the LSPR linewidth variation in our nanorods is solely due to the varying contribution from radiation damping.

2. Synthesis and etching of gold nanorods:

We first synthesized three Au nanorods following protocols already reported in the literature. In the next step, we used H_2O_2 mediated controlled etching to alter the lengths of these as prepared Au nanorods to achieve NR1, NR2 and NR3, which have the exact structural and optical specifications required for our work. We call as-prepared Au nanorods as 'precursor nanorod' of NR1/ NR2/ NR3.

(a) Synthesis of precursor nanorod of NR1: The precursor nanorod of NR1 was synthesized following previously reported[3] two-step method. In the first step, Au^{3+} is reduced by a strong reducing agent, $NaBH_4$, to form gold seed. Thus prepared seed is then added to the growth solution to obtain the nanorods. The details of both the steps are discussed below.

Seed preparation (First step): 5 ml Au^{3+} solution (0.5 mM) was added to 5 ml of 0.2 M CTAB solution followed by addition of ice cold 0.01 M $NaBH_4$ (0.6 ml). The solution was stirred vigorously for 2 min and kept undisturbed for 2 h at 25 ^oC.

Nanorod growth (Second step): Growth solution was prepared by adding 5 ml Au^{3+} (1 mM) to 5 ml of CTAB (0.2 M) solution. To this mixture, 200 μl $AgNO_3$ (4 mM) and 70 μl of ascorbic acid (0.0788 M) was added and the mixture was shaken gently. At the end, 12 μl of seed was added and solution was kept undisturbed for 24 hours at 27 °C -29 °C.

(b) Synthesis of precursor nanorods of NR2 and NR3: The precursor nanorods of NR2 and NR3 were prepared by previously reported[4] one-pot synthesis protocol. A weak reducing agent, pyrogallol (1,2,3 trihydroxybenzene), was used in this case. Two identical sets of reaction mixtures, each comprising of 0.1 M aqueous CTAB solution, 0.4 mM aqueous $HAuCl_4$ solution, and 0.36 mM 1,2,3 trihydroxybenzene solution, were prepared. Next, 0.045 mM and 0.070 mM aqueous $AgNO_3$ solutions were added to set-1 and set-2, respectively. The volume of the mixture in each set was made up to 7.6. ml. Next, 0.0039 mM $NaBH_4$ was added to each of the sets to initiate the reaction. Reaction mixture was kept undisturbed for 24 hours at 27°C - 29°C. Set-1 and set-2 yielded the precursors of NR2 and NR3 respectively.

Etching of precursor nanorods: The LSPR maxima of as-synthesized nanorods were far from the resonance of TDBC J-band. For example, the LSPR maxima of the precursors of NR1, NR2 and NR3 were at 663 nm, 768 and 698 nm, respectively. In order to bring the LSPR at J-band position, as-prepared Au nanorods were etched[5] using hydrogen peroxide (H_2O_2, 30% v/v). The amount of H_2O_2 used for etching was optimized according to the diameter of nanorods. After adding H_2O_2, the solutions were heated to initiate etching of the nanorods and the etching process was monitored by monitoring the extinction spectra as a function of time, as shown in Figure S1.

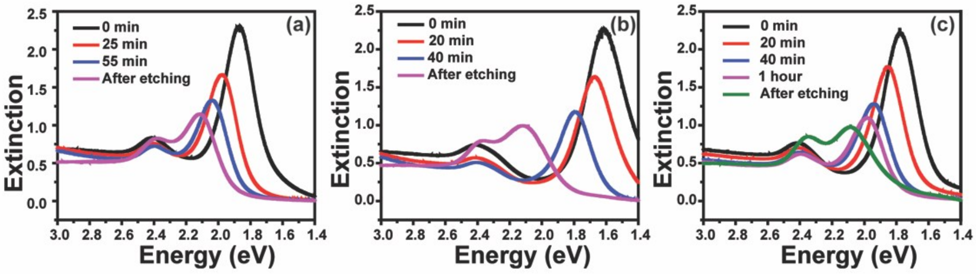

Figure S1. Extinction spectra showing time dependence of hydrogen peroxide mediated etching of the precursor nanorods of (a) NR1, (b) NR2 and (c) NR3. Each etching reaction is immediately quenched once the desired LSPR wavelength is achieved.

For preparing NR1, 80 μl of H_2O_2 was added to 1 ml of precursor nanorod solution and the reaction was quenched by centrifuging the solution at 10000 rpm and discarding the supernatant. For preparing NR2 and NR3, the added amount of H_2O_2 were 400 and 700 μl, respectively and centrifugation speeds of 8000 and 6000 rpm were used to quench the reactions. After centrifugation, supernatants were discarded and the residues were redispersed in 1 ml 0.1 M CTAB. These solutions (NR1/NR2/NR3) were used for further study.

3. Preparation of plexcitonic hybrid:

TDBC molecule is negatively charged while the Au NR's surface is covered with positively charged CTAB. Therefore, TDBC molecule and Au NR's surface is expected to interact via electrostatic attraction. A stock solution of 1 mM of TDBC in water was prepared and used within 48 hours after preparation. 200 μl aliquots of the TDBC stock solution were added to 800 μl of NR1/ NR2/NR3 solutions. These solutions were kept undisturbed for 24 h. This step was followed by the removal of excess (unbound) monomer by centrifugation. The centrifugation speed of 10000, 8000, 6000 rpm were selected for NR1, NR2 and NR3, respectively. The obtained residue was again dispersed in water for further study.

4. Characterization of Gold Nanorods:

Physical dimension of gold nanorods were characterized using scanning electron microscopy (SEM). Figures S2 (a-c) show representative SEM micrographs of NR1, NR2 and NR3. The average dimensions of these etched gold nanorods and their resonance energies are listed in Table1 of the main manuscript. Figure S3 represents the statistical distribution of length, width (diameter) and aspect ratio of all the nanorods obtained from SEM analyses.

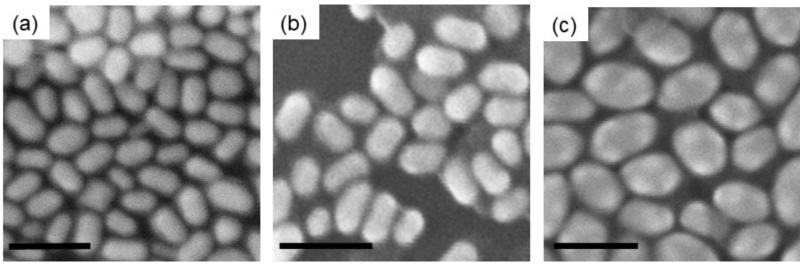

Figure S2. SEM images of three different nanorods (a) NR 1 (b) NR 2 (c) NR 3. Each of the scale bar refers to 100 nm.

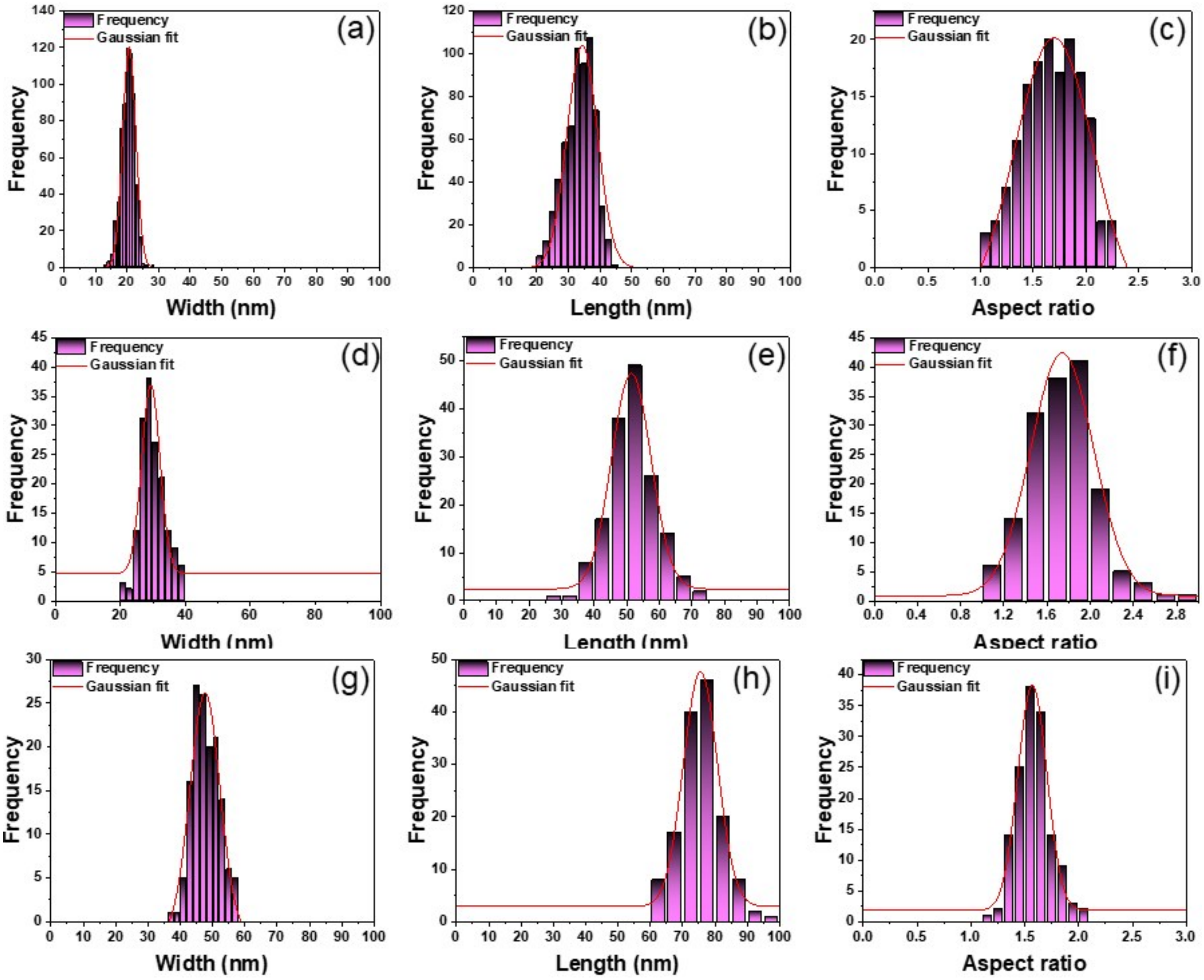

Figure S3. Statistical distribution histograms for different size parameters of NR1-NR3 are shown. The top, middle and bottom panels refer to NR1, NR2 and NR3, respectively. Width distribution histograms are shown in(a,d and g), length distribution histograms distribution histograms are shown in (b,e and h) and aspect ratio distribution histograms distribution histograms are shown in (c, f and i).

5. Dark field scattering spectroscopy of gold nanorods and J-aggregates:

Single particle scattering spectra of gold nanorods and their plexcitonic hybrids were obtained by using Nikon Ti2E inverted microscope coupled to a spectrometer and a camera. Diluted samples were dropcasted on patterned glass slides and dried under nitrogen. Nanorods were well dispersed on the glass slides. The samples were excited by broadband white light from a halogen light source. A dry dark field condenser (Nikon, numerical aperture (NA) = 0.80-0.95), oriented normal to glass surface, was used to focus the white light onto the sample. Scattered light from individual particle was collected using a dry objective (60x, 0.70 NA) and finally focused onto the entrance slit of spectrometer (Kymera, Andor). The spectrometer was equipped with an interchangeable diffraction grating (600 grooves/mm) and reflecting mirror, which helped in acquiring the image as well as the spectrum of a particle. The images and spectra were recorded using a scientific complementary metal oxide semiconductor (sCMOS) detector (Zyla, Andor Technology) which was attached to the exit slit of the spectrometer. Position of entrance slit in spectrometer at the image plane helped in projecting the scattered light to the detector, enabling the wide-field image of dark field scattering from the nanoparticles. After acquiring the wide-field image, scattering spectra of a particle of interest is recorded by adjusting the slit width. Each recorded spectrum was corrected for all background noises. 30-40 single particle spectra were collected for each sample and analyzed. A schematic of the experimental set up for dark field scattering is shown in Figure S4.

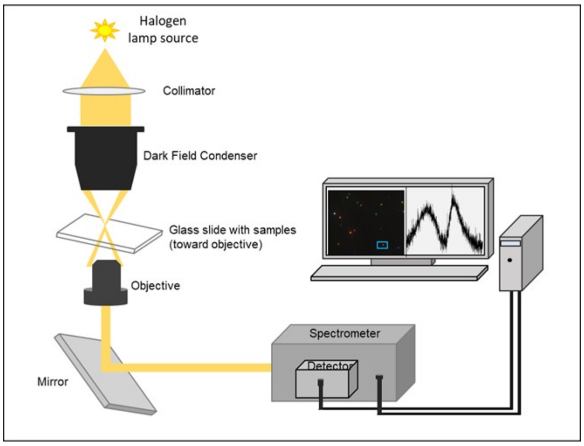

Figure S4. Schematic of the experimental set-up for dark-field scattering microspectroscopy**.**

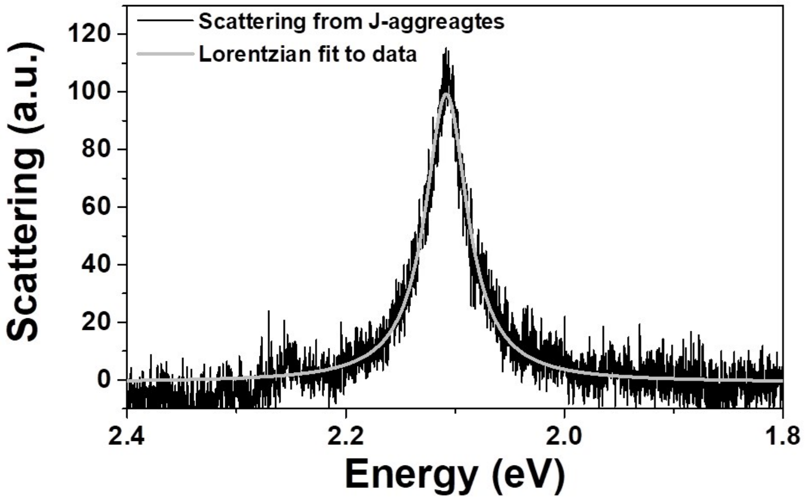

Figure S5. Dark-field scattering spectrum of J-aggregates on glass slide. A single Lorentzian describes the spectrum quite convincingly.

Scattering spectra of J-aggregates can be fitted quite satisfactorily with single Lorentzian function. This implies insignificant contribution of inhomogeneous broadening toward the overall spectral linewidth. Such an adequate fitting has two implications: (1) pure Lorentzian behaviour of both exciton and LSPR resonances allow us to use coupled harmonic oscillators model to describe our polariton system, and (2) negligible contribution of inhomogeneous broadening to the scattering spectrum of J-aggregates is suggestive of absence of any significant structural disorder in the J-aggregates studied here.

6. Numerical simulation:

Numerical simulation of Au nanorods and Au nanorod-TDBC composite was carried out using finite difference time domain (FDTD) technique. A commercially available software package “FDTD solutions v8.12”(Lumerical) was used for this purpose. A detailed discussion of the methods of numerical simulation of the optical properties of plasmonic and plexcitonic nanostructures can be found in our previous publications.[6,7] The solver-defined total-field scattered-field (TFSF) that allows the definition of the plane-wave excitation within the volume enclosing only the simulation objects was used as light source. The direction of propagation and the plane of polarization of light was chosen to be perpendicular and parallel to the long axis of nanorod (or hybrid), respectively. Frequency dependent absorption and scattering cross sections were calculated by six two-dimensional monitors (frequency domain field and power monitors) placed in a cubic fashion around the nanorod (or hybrid). One two-dimensional monitor was placed in XY plane to calculate the average intensity of electric field. Time monitor was used to calculate electric field intensity as a function of time. Mesh accuracy of 5 was used for the simulation. A cubic mesh of 1 nm length was used for the simulation of absorption and scattering spectra while a meshing of 0.25 nm × 0.25 nm × 0.5 nm was employed for calculating the electric field distribution. The simulation was carried out on single Au nanorod (or J-aggregate coated Au nanorod). The size parameters of the particles used in the simulation were taken from result of the actual SEM analyses. The refractive index of the surrounding medium was taken as 1.33 to mimic aqueous environment. For simulating the absorption spectra of nanorod plexcitons, the complex dielectric permittivity of the TDBC J-aggregate covering the Au nanorod was modelled using the single Lorentzian function,[8,9]

$$\varepsilon_{\infty}(\omega) = \varepsilon_{\infty} + \frac{f\omega_e^2}{(\omega_e^2 - \omega^2 - i\gamma_e\omega)}$$

(2)

Where, ε_∞ =1.5 is high frequency component of J-aggregates of TDBC dye layer; f = 0.015 is the reduced oscillator strength of dye layer; $\omega_e = 2.13\ eV$ is the exciton resonance, which has been kept fix for all the Au nanorod-dye composites; $\gamma_e = 30\ meV$ is the spectra linewidth of the exciton (J-band). The absorption spectra of the plexciton hybrids of NR1, NR2 and NR3 are shown in Figure S5.

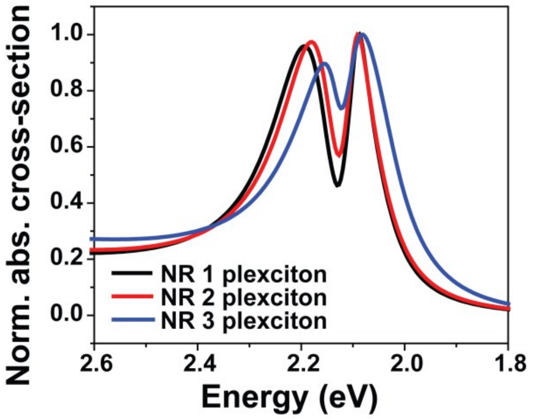

Figure S6. Normalized absorption spectra of the Au nanorod-TDBC J-aggregate hybrids obtained through numerical simulation using FDTD technique. Decrease in Rabi-splitting energy as well as the depth of transparency dip, from NR1 to NR3, is quite obvious.

7. Contribution of absorption and scattering in the extinction spectra of Au NRs

As mentioned in the main text, a preliminary indication of whether strong coupling is possibly being operational in a plexciton system is obtained when mode-splitting is observed both in the absorption as well as the scattering spectra. In absence of pure absorption spectrum, one can rely on the extinction spectral measurement provided the extinction spectrum is dominated by absorption. The presented ensemble averaged spectra (Figure 1 of the main manuscript) of Au nanorods are extinction spectra in true sense and the extinction spectra will have some contribution from scattering. To find out whether or not the extinction spectra of our Au NRs and Au NR plexciton hybrids are dominated by absorption, we resorted to numerical simulation using FDTD method as described in section 6 above. FDTD simulations reveal that for the Au nanorods studied in this work, the absorption cross-sections are much larger than the scattering cross-sections. The FDTD simulated spectra (extinction, absorption and scattering) for NRs are shown in Figure S7 (top panels). The corresponding simulated spectra of NR-plexcitons are also shown (bottom panel). It is quite clear from Figure S7 that absorption contribution is overwhelmingly dominant in the extinction spectra. Moreover, when we look at the corresponding plexciton spectra (bottom panel), the dip intensity of absorption and extinction are quite comparable while the contribution of scattering to the overall extinction is very small. A comparison of the experimental extinction spectra (Figure 1 in the main manuscript) with the theoretical spectra presented in Figure S7 tells us that the mode splitting with prominent dip in the experimental extinction spectra predominantly arises from absorption spectral contribution. Thus, our extinction measurements and analyses indirectly, yet convincingly, prove that plexciton dip is indisputably present in the absorption spectra of Au NR-J-aggregate hybrids. In other words, our experimental (ensemble level extinction measurement and single particle scattering measurements) results and numerical analyses are convincing enough to prove that mode-splitting with intense transparency dip occur both in absorption as well as in scattering spectra of the Au nanorod-J-aggregate hybrids. This is the only information that is relevant for the present work. However, it is important to note here that if a plexciton system satisfy this criteria then it is just an indication of possible strong coupling but not a unequivocal proof, which requires that the condition $2g \gg \sqrt{\gamma_p \gamma_e}$ is met. As a matter of fact we showed that NR3 does not qualify for strong plexciton coupling category in spite of showing mode splitting in both extinction (absorption dominates) and scattering spectra along with mode anti-crossing behaviour.

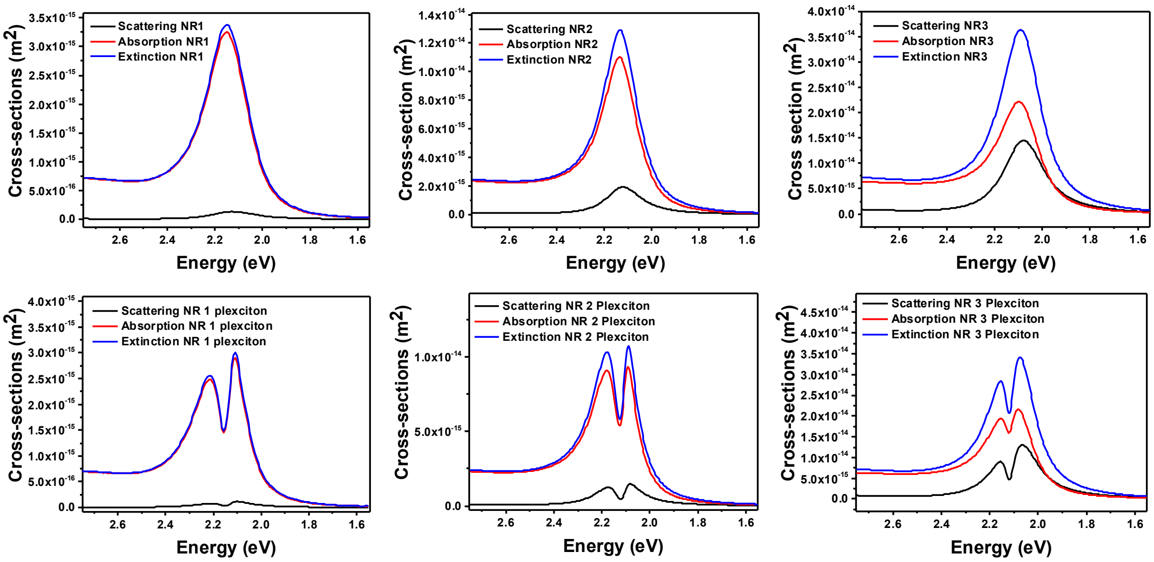

Figure S7. FDTD simulated extinction, absorption and scattering spectra of the Au nanorods (top panel) and Au nanorod-TDBC J-aggregate hybrids (bottom panels) are shown. Dominance of the absorption contribution over scattering in the extinction is quite obvious.

8. Determination of linewidth in ensemble average extinction spectra

We extracted the linewidths of the spectra presented in in Figure 1 (a) of the main manuscript by multi-peak fitting using Origin Pro 9.1 software. For this, we considered the contributions from (i) Interband transitions, (ii) transverse mode of nanorods and (iii) the longitudinal mode of nanorods. As only the longitudinal mode is relevant to us, we analyze (using Origin Pro) the fitted longitudinal mode of nanorod and extract its linewidth. The peak fitting analyses for the extinction spectra of Au NR are shown in Figure S8. In a very similar way, we fit every single-particle scattering spectrum with a single Lorentzian peak function using Origin Pro 9.1 software and extract the corresponding LSPR spectral linewidth. The fitted curves for scattering data are already there in the Fig. 2 of the main manuscript.

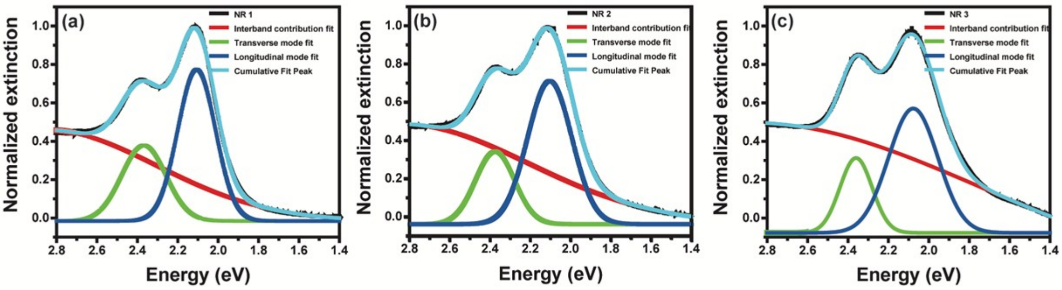

Figure S8. Multi peak fitting analyses of the extinction spectra of the Au NRs are shown. The fitted longitudinal mode of each nanorod system is analyzed using Origin Pro software and the corresponding linewidth is extracted.

9. An alternate measure of mode-volume and comparing it with geometrical volume

As mentioned in the main text, mode-volume determines the confinement of electric field in a cavity. In the classical picture of coupled oscillators involving a cavity and an exciton, the cavity mode volume characterizes electric field confinement at the exciton position. In the main text, we have explicitly mentioned this concept of mode-volume for dissipative and highly dispersive materials and also referred to the mathematical formulation for its estimation (Equation 3). However, we also categorically described the rationale behind adopting Purcell's concept of treating geometrical volume as the mode volume for sub-wavelength open cavities like Au NRs. As a matter of fact, treating geometrical volume as the mode volume for sub-wavelength open cavities is the most common and well accepted practice.

Nevertheless, instead of the total volume of the nanorods, the optical field 'skin' that encompasses the nanoparticle and interact with the molecular exciton layer can be considered as an alternative measure of the cavity mode volume. In a way, expressing mode-volume in this manner rather closely resembles the concept provided by equation 3. Therefore, in this section, we additionally express the mode-volume of our plasmonic cavity as the volume of the thin shell of dye encompassing the NR (as opposed to total volume of NR). Subsequently, we examined whether expressing mode-volume in this manner alter the dependency of Rabi splitting on mode-volume as depicted in Figure 4b of the main manuscript. The corresponding plot of the Rabi splitting vs modified mode volume(i.e., dye layer volume) is shown in Figure S9. is also shown on the right. Comparing Figure S9 with Figure 4b, we can see that the nature of the two plots are very similar and therefore, the redefining the mode-volume does not change the interpretation of the data presented in Figure 4b. Also, this result indicates that expressing the mode-volume of any plasmonic open cavity as the volume of the thin shell of molecular exciton encompassing the NR can be an excellent alternative to the Purcell's concept of mode-volume. More importantly, this will prove extremely beneficial particularly in case of very large nanoparticles for which Purcell's definition does not work as it unrealistically overestimates the mode-volume.

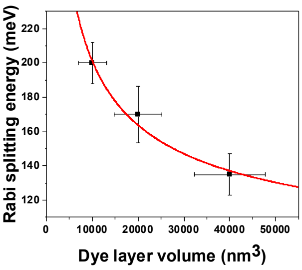

Figure S9. Variation of Rabi splitting energy when the mode-volume id expressed as the volume of the dye layer encompassing the nanorod.

7.References

S1 B. Foerster, A. Joplin, K. Kaefer, S. Celiksoy, S. Link and C. Sönnichsen, *ACS Nano*, 2017, **11**, 2886–2893.

S2 M. Hu, C. Novo, A. Funston, H. Wang, H. Staleva, S. Zou, P. Mulvaney, Y. Xia and G. V. Hartland, *J. Mater. Chem.*, 2008, **18**, 1949.

S3 B. Nikoobakht and M. A. El-Sayed, *Chem. Mater.*, 2003, **15**, 1957–1962.

S4 L. Zhang, K. Xia, Z. Lu, G. Li, J. Chen, Y. Deng, S. Li, F. Zhou and N. He, *Chem. Mater.*, 2014, **26**, 1794–1798.

S5 W. Ni, H. Chen, J. Su, Z. Sun, J. Wang and H. Wu, *J. Am. Chem. Soc.*, 2010, **132**, 4806–4814.

S6 B. Hazra and M. Chandra, *ACS Sens.*, 2016, **1**, 536–542.

S7 K. Das, B. Hazra and M. Chandra, *Phys. Chem. Chem. Phys.*, 2017, **19**, 27997–28005.

S8 A. E. Schlather, N. Large, A. S. Urban, P. Nordlander and N. J. Halas, *Nano Lett.*, 2013, **13**, 3281–3286.

S9 G. Zengin, G. Johansson, P. Johansson, T. J. Antosiewicz, M. Käll and T. Shegai, *Sci. Rep.*, 2013, **3**, 3074.